Identification of the inhibitory mechanism of FDA approved selective serotonin reuptake inhibitors: an insight from molecular dynamics simulation study†

Weiwei Xue,[a] Panpan Wang,[a] Bo Li,[a] Yinghong Li,[a] Xiaofei Xu,[a] Fengyuan Yang,[a] Xiaojun Yao,[b] Yu Zong Chen,[c] Feng Xu*[d] and Feng Zhu*[a]

Antidepressants selectively inhibiting serotonin reuptake (SSRIs) represent a highly effective drug class, and novel therapeutic strategies were proposed to improve SSRIs' drug efficacy. The knowledge of the inhibitory mechanism of FDA approved SSRIs could provide great insights and act as important starting points to discover privileged drug scaffolds with improved efficacy. However, the structure of human serotonin transporter (hSERT) is yet to be determined and the inhibitory mechanism underlying SSRIs still needs to be further explored. In this study, the inhibitory mechanism of 4 approved SSRIs treating major depression (fluoxetine, sertraline, paroxetine and escitalopram) was identified by integrating multiple computational methods. Firstly, a recently published template with high sequence identity was adopted for the first time to generate hSERT's homology model. Then, docking poses of 4 SSRIs were used as the initial conformation for molecular dynamics (MD) simulation followed by MM/GBSA binding free energy calculation and per-residue free energy decomposition. Finally, the binding mode shared by the 4 studied SSRIs was identified by hierarchically clustering per-residue free energies. The identified binding mode was composed of collective interactions between 3 chemical groups in SSRIs and 11 hot spot residues in hSERT. 6 out of these 11 were validated by previous mutagenesis studies or pharmacophore models, and the remaining 5 (Ala169, Ala173, Thr439, Gly442 and Leu443) found in this work were not yet been identified as common determinants of all the 4 studied SSRIs in binding hSERT. Moreover, changes in SSRIs' binding induced by mutation on hot spot residues were further explored, and 3 mechanisms underlining their drug sensitivity were summarized. In summary, the identified binding mode provided important insights into the inhibitory mechanism of approved SSRIs treating major depression, which could be further utilized as a framework for assessing and discovering novel lead scaffolds.

[a] *Innovative Drug Research and Bioinformatics Group, Innovative Drug Research Centre and College of Chemistry and Chemical Engineering, Chongqing University, Chongqing 401331, China. E-mail: zhufeng@cqu.edu.cn*

[b] *State Key Laboratory of Applied Organic Chemistry and Department of Chemistry, Lanzhou University, Lanzhou 730000, China*

[c] *Bioinformatics and Drug Design Group, Department of Pharmacy, National University of Singapore 117543, Singapore*

[d] *College of Pharmacy and Tianjin Key Laboratory of Molecular Drug Research, Nankai University, Tianjin 300071, China. E-mail: xufeng@nankai.edu.cn*

† Electronic supplementary information (ESI) available. See DOI: 10.1039/c5cp05771j

Introduction

Antidepressants inhibiting serotonin reuptake represent a highly effective class of therapeutics treating major depression and generalized anxiety disorder,[1] and are the first-line and the most prescribed class of antidepressants in the United States.[2]

Typical antidepressants of this class include selective serotonin reuptake inhibitors (SSRIs), serotonin–norepinephrine reuptake inhibitors (SNRIs)[3] and others.[4–7] So far, this class has >10 marketed antidepressants approved by U. S. Food and Drug Administration (Fig. 1) and several candidates in clinical trial. As the primary target of SSRIs,[8,9] human serotonin transporter (hSERT) plays a key role in regulating the duration and intensity of the serotonin signal in the synaptic cleft,[10] and is thus closely related to the pathology of mood and anxiety disorders.[11]

In order to deal with the delayed onset of action[12] and the partial- or non-response[13] of SSRIs treating depression, novel therapeutic strategies were frequently proposed as an "improvement" to the drug efficacy.[14,15] These strategies include designing dual- and triple-acting antidepressants,[15] multi-targeting hSERT and acid sphingomyelinase,[16] enhancing SSRIs' efficacy by co-targeting the low-affinity high-capacity hSERT,[17] and others.[18,19] The binding mode of certain SSRIs to hSERT was
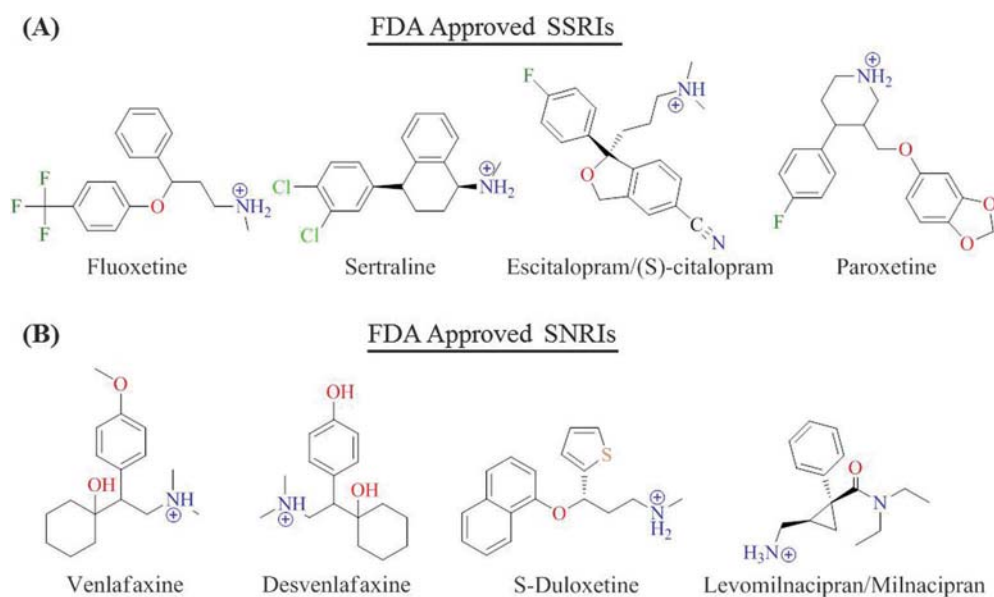
Fig. 1 Structures of the SSRI and SNRI antidepressants approved by FDA.

reported to be crucial for revealing its specific inhibitory mechanism and drug efficacy.[20–22] A detailed understanding of the binding mode shared by SSRIs of clinical importance, especially FDA approved 4 SSRIs (Fig. 1), could provide more insights into the identification of privileged drug-like scaffolds with improved drug efficacy.[21,23]

The determination of the crystal structure of hSERT's bacterial homolog LeuT[24,25] provided a template to elucidate the binding mode of SSRI–hSERT *via* computational methods[26] in the past decade. The most frequently used methods include induced fit docking (IFD),[20–22,27,28] pharmacophore model[29–31] and molecular dynamics (MD).[32] IFD focuses on considering the flexibility of hSERT's amino acid side chains lining the binding cavity,[27] while the pharmacophore model is primarily designed for screening new SSRIs.[31] For a better mobile recognition mechanism of SSRI–hSERT, MD simulation was used to reveal the binding of substrates and drugs to hSERT's S1 site,[26,33–35] a reported primary binding site for SSRIs' competitive inhibition.[36–38] However, so far escitalopram has been the only approved SSRI, the binding mode of which to the S1 site was analyzed by MD simulation.[32,39] Currently, no comprehensive study on binding modes of SSRIs–hSERT has been carried out. Thus, a detailed understanding of the inhibitory mechanism underlining SSRIs' pharmacological activity and target recognition is in urgent need.[20,36]

In this study, we carried out an inhibitory mechanism identification of 4 FDA approved SSRIs treating major depression (fluoxetine, sertraline, paroxetine and escitalopram) by integrating multiple computational methods. Firstly, a newly reported template of Drosophila dopamine transporter (dDAT)[36] with much higher sequence identity (53%) than LeuT (23%) was used for the first time to generate the homology model of hSERT. Then, SSRIs were docked into hSERT and used as the initial conformation for MD simulation. Finally, a binding mode (at the atomic level)

shared by the 4 studied SSRIs was identified by clustering per-residue binding free energies. As a validation, drug sensitive mutations inducing >10-fold shifts on inhibitory potency (K_i)[40] were further explored. The binding mode identified in this study provided important insights into the inhibitory mechanism of approved SSRIs, which could be further utilized as a useful framework for assessing and discovering novel lead scaffolds.[23]

Methods

Homology modeling

As illustrated in Fig. S1, ESI† a recently determined 3.0 Å X-ray crystal structure (PDB code 4M48[36]) of dDAT (from Glu26 to Asp599) showed a much higher sequence identity (53%) to hSERT compared to LeuT[24] (23%). By using it as template, the automated mode in SWISS-MODEL[41] was applied to construct a homology model of hSERT. The constructed model was from Glu78 to Pro617, which covers all 12 transmembrane regions and the corresponding intervening loops. Then, the Ramachandran plot in PROCHECK[42] was applied to validate the constructed model. Finally, two functional Na^+ in LeuBAT[37] (a LeuT variant engineered to harbor hSERT-like pharmacology by mutating key residues around the primary binding pocket) were manually fitted into their corresponding binding sites in hSERT *via* PyMOL's[43] structure superimposition.

Molecular docking

To get their initial poses, 4 SSRIs were docked into the modeled hSERT using Glide[44] with standard precision. Residues identified as key determinants of SSRI–hSERT binding[21,40] were used to define the docking grid box. Docking poses of fluoxetine, sertraline and paroxetine with the most similar conformations as those in LeuBAT[37] and the docking pose of escitalopram

This journal is © the Owner Societies 2016

Phys. Chem. Chem. Phys., 2016, **18**, 3260–3271 | **3261**

with the most similar orientation as those of fluoxetine, sertraline and paroxetine were selected as their initial binding poses for MD simulation. Moreover, to assess the validity of the docking approach in the studied model, a cross-docking strategy was adopted by docking a SSRI into the structure of LeuBAT obtained with other SSRI-bound (*e.g.* docking fluoxetine into the structure of LeuBAT obtained with sertraline-bound). The co-crystallized poses of fluoxetine, sertraline and paroxetine (PDB codes 4MM8, 4MM5 and 4MM4) in LeuBAT[37] were superimposed onto their corresponding cross-docking poses. Although, no co-crystallized structure of escitalopram in LeuBAT has been reported, its resulting docking pose is oriented in a very similar way as fluoxetine, sertraline and paroxetine in LeuBAT, which forms an ionic interaction between the ammonium group and the residue Asp98. The detailed information can be found in ESI,† Methods.

Protein–ligand/membrane system setup

SSRI–hSERT complexes obtained by docking were embedded into the explicit POPC lipid bilayer using the Membrane Builder in CHARMM-GUI.[45–47] TIP3P water[48] of 20 Å thickness was then placed above and below the constructed bilayer. The environmental salt concentration was kept at 0.15 M by adding Na^+ and Cl^-. The overall system contained a total of $\sim 96\,000$ atoms per periodic cell, and the box size was set to $83 \times 83 \times 127$. The detailed information can be found in ESI,† Methods.

MD simulation

MD simulation was performed within AMBER14[49] using GPU-accelerated PMEMD. AMBER force field *ff14SB*[50] and *Lipid14*[51] were used for proteins and lipids, respectively. The ion parameters of TIP3P water were collected from Joung & Cheatham.[52] The force field parameters of fluoxetine, sertraline, escitalopram, paroxetine and cholesterol were described by the General AMBER Force Field[53] and the charges were assigned using restrained electrostatic potential partial charges[54] with antechamber.[55] Geometry optimization and the electrostatic potential calculations were performed using Gaussian09 at the HF/6-31G* level.[56] For each simulation, a sophisticated protocol including minimization, heating and equilibration was employed. Then, 150 ns MD simulation was performed in an NPT ensemble at a temperature of 310 K and a pressure of 1 atm using a periodic boundary condition. Meanwhile, the direct space interaction was calculated by considering the long range electrostatic interaction (cutoff = 10.0 Å) using the particle-mesh Ewald method.[57] All bonds involving hydrogen were constrained by the SHAKE algorithm[58] allowing an integration time step of 2 fs. The detailed information can be found in ESI,† Methods.

Binding free energy calculation

Binding free energy ($\Delta G_{\text{MM/GBSA}}$) of SSRIs to hSERT excluding entropic contribution was calculated using the single-trajectory based MM/GBSA method.[59,60] A total of 500 snapshots were taken from the last 50 ns MD simulation. For each snapshot, the SSRI–hSERT binding free energy was calculated using

$$\Delta G_{\text{MM/GBSA}} = \Delta E_{\text{vdW}} + \Delta E_{\text{ele}} + \Delta G_{\text{pol}} + \Delta G_{\text{nonpol}} \qquad (1)$$

In eqn (1), ΔE_{vdW} and ΔE_{ele} are the van der Waals and electrostatic components in the gas phase, and ΔG_{pol} and ΔG_{nonpol} are the polar and non-polar solvent interaction energies. ΔG_{nonpol} was calculated using $\Delta G_{\text{nonpol}} = 0.0072 \times \Delta \text{SASA}$ by the linear combination of the pairwise overlap (LCPO) method,[61] where SASA is the solvent accessible area. The detailed information can be found in ESI,† Methods.

Per-residue free energy decomposition analysis

To quantitatively evaluate the contribution to SSRI binding, the total binding free energy was decomposed on a per-residue basis. The corresponding binding free energy ($\Delta G_{\text{MM/GBSA}}^{\text{per-residue}}$) excluding entropic contribution was given by:

$$\Delta G_{\text{MM/GBSA}}^{\text{per-residue}} = \Delta E_{\text{vdW}}^{\text{per-residue}} + \Delta E_{\text{ele}}^{\text{per-residue}} + \Delta G_{\text{pol}}^{\text{per-residue}}$$
$$+ \Delta G_{\text{nonpol}}^{\text{per-residue}} \qquad (2)$$

The definition of quantities in eqn (2) is similar to that in eqn (1), except for the non-polar solvent interaction energy ($\Delta G_{\text{nonpol}}^{\text{per-residue}}$) which is calculated using the recursive approximation of a sphere around an atom, starting from an icosahedron (ICOSA).[49] The detailed information can be found in ESI,† Methods.

Hierarchical clustering with the Ward algorithm

Energy contributions of certain residues to the 4 studied SSRIs calculated in the previous section were used to generate a 4-dimensional vector. Then, the per-residue energy contribution vector-based hierarchical clustering tree of 245 residues with contributions to at least one studied SSRI in hSERT's binding (contribution $\neq$ 0 kcal mol^{-1}) was generated using R statistic analysis software[62] with the similarity levels among vectors measured by the Manhattan distance:

$$\text{Distance } (a, b) = \sum_i |a_i - b| \qquad (3)$$

where i denotes each dimension of per-residue energies a and b. The cluster algorithm used here is Ward's minimum variance method,[63] which is designed to minimize the total within-cluster variance. In this study, a Ward's minimum variance module in R package was used.[62] The hierarchical tree graph was generated using EMBL's online tree generator (iTOL[64] version 3.0). Per-residue binding free energy contributions favoring SSRI's binding were displayed in red, with the highest contribution set to exact red and lower contributions gradually fading towards white (no contribution). Meanwhile, per-residue energy contributions hampering SSRI's binding were shown in blue, with the highest one set to exact blue and the lower ones gradually fading towards white.

Results and discussion

Homology modeling and SSRI–hSERT complex construction

As shown in Fig. S2, ESI† superimposition of the modeled hSERT and the X-ray crystal structure of dDAT[36] showed a high

degree of homology. The structure of modeled hSERT consists of 12 transmembrane α-helices, and the corresponding residues within these helices agree well with the reported experimental results.[65] The stereochemical quality and accuracy of the predicted model was evaluated by the Ramachandran plot in PROCHECK,[42] and 99.5% of the modeled residues were located in the "allowed region" (ESI,† Fig. S3), indicating a reliable homology model.

Based on the modeled hSERT, molecular docking was carried out to determine initial poses of SSRIs in hSERT. The results (ESI,† Fig. S4) show that fluoxetine, sertraline, escitalopram and paroxetine fit in the binding site primarily surrounded by TM1, TM3, TM6 and TM8. To assess the validity of the docking approach in the studied model, a cross-docking strategy was adopted by docking SSRIs into the structure of LeuBAT obtained with other SSRI-bound (for example, docking fluoxetine into the structure of LeuBAT obtained with sertraline-bound). The co-crystallized poses of fluoxetine, sertraline and paroxetine (PDB codes 4MM8, 4MM5 and 4MM4) in LeuBAT[37] were superimposed onto their corresponding cross-docking poses. Both poses were kept consistent with each other (ESI,† Fig. S5), which guaranteed the correct initial poses generated in this work. So far, no co-crystallized structure of escitalopram in LeuBAT has been reported, but its resulting docking pose is oriented in a very similar way as fluoxetine, sertraline and paroxetine in LeuBAT, which forms an ionic interaction between the ammonium group and the residue Asp98.

Assessing the binding mode of SSRI–hSERT

Simulation stability analysis. The initial SSRI–hSERT complex generated by docking was assessed by 150 ns MD simulation to reach the equilibration state, which could be monitored by the structural root mean square deviation (RMSD) of both protein backbone atoms and ligand heavy atoms as a function of time. According to RMSD analysis (Fig. 2), each simulation of hSERT in complex with the 4 studied SSRIs reached equilibration around 100 ns, and a time scale of 150 ns was therefore set in this work to guarantee a stable state for the SSRI–hSERT complex.

Binding free energy analysis. Binding free energies of hSERT in complex with fluoxetine, sertraline, escitalopram and paroxetine were calculated, and the results ($\Delta G_{\text{MM/GBSA}}$) were −41.52, −44.32, −49.21 and −51.14 kcal mol^{-1} respectively. Meanwhile, experimental binding free energies (ΔG_{exp}) were also estimated based on the reported K_i values[40] using $\Delta G_{\text{exp}} = -RT\ln(K_i)$. As shown in Table 1, $\Delta G_{\text{MM/GBSA}}$ values in this work were overestimated compared to those of experiment.[40] For ligands with similar structures and binding modes, entropy contribution could be omitted if one is only interested in the relative order of binding affinities,[66] so differences in energies calculated in this study ($\Delta\Delta G_{\text{MM/GBSA}}$) and estimated based on experiments ($\Delta\Delta G_{\text{exp}}$) among SSRIs (Table 1) could help understand whether the overestimation came from the exclusion of entropy. As illustrated in Fig. S6, ESI† $\Delta\Delta G_{\text{MM/GBSA}}$ correlates very well with $\Delta\Delta G_{\text{exp}}$ ($R^2 = 0.93$). The ascending trend of energy difference ($\Delta\Delta G_{\text{exp}}$) from experiment[40] was reproduced very well by $\Delta\Delta G_{\text{MM/GBSA}}$ in this work, though their values were still estimated higher than experiment.[40] The higher energy calculated in this work was in accordance with the reported overestimation of binding affinity by the MM/GBSA methods.[67–69] Calculated contributions of each energy term in eqn (1) are listed in Table S1, ESI.† As shown by numbers in bold, the
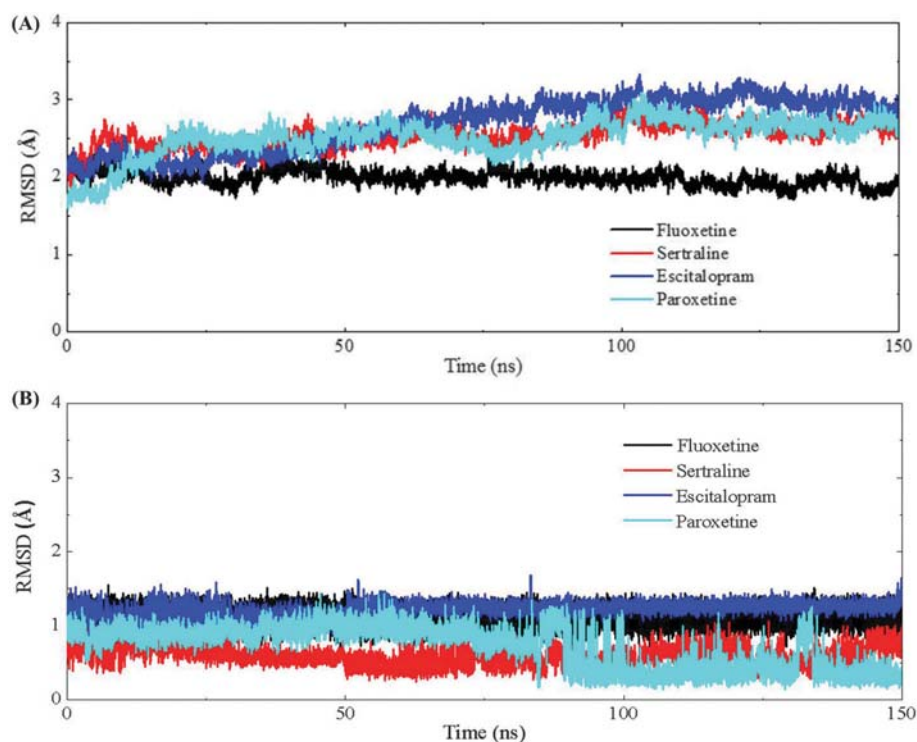

Fig. 2 Root mean square deviations of protein backbone atoms (A) and ligand heavy atoms (B) as a function of time in MD simulations.

This journal is © the Owner Societies 2016

Phys. Chem. Chem. Phys., 2016, **18**, 3260–3271 | **3263**

Table 1   Comparison between the calculated and experimental binding free energies among the 4 studied SSRIs to the wild type hSERT (ΔG is in kcal mol^{-1} and K_i value is in nM)

Systems	$K_i{}^{a}$	$\Delta G_{exp}{}^{b}$	$\Delta\Delta G_{exp}$	$\Delta G_{MM/GBSA}{}^{c}$	$\Delta\Delta G_{MM/GBSA}$
Fluoxetine	255 ± 61	-9.00	0	-41.52 ± 0.10	0
Sertraline	242 ± 33	-9.03	-0.03	-44.32 ± 0.12	-2.80
Escitalopram	32 ± 1	-10.23	-1.23	-49.21 ± 0.12	-7.69
Paroxetine	24 ± 6	-10.40	-1.40	-51.14 ± 0.12	-9.62

[a] Experimental value from Sørensen's work.[40] [b] Estimated binding free energy based on K_i values using $G_{exp} = -RT\ln(K_i)$. [c] Calculated binding free energy in this work.

binding of SSRIs to hSERT was primarily driven by hydrophobic (ΔE_{vdW}) and coulomb interaction energies (ΔE_{ele}), but hampered by the polar solvent energy (ΔG_{pol}).

Analyzing the binding mode of SSRI–hSERT. In this study, the binding mode of each SSRI–hSERT was obtained by molecular docking and further assessed by MD simulation. As illustrated in Fig. S7 (ESI†), slight conformation shifts between 4 SSRIs' docking poses and their representative snapshots in the equilibrated MD trajectories were observed, but the key interactions such as the salt bridge and the hydrogen bond between the ligands and Asp98 of hSERT were preserved.
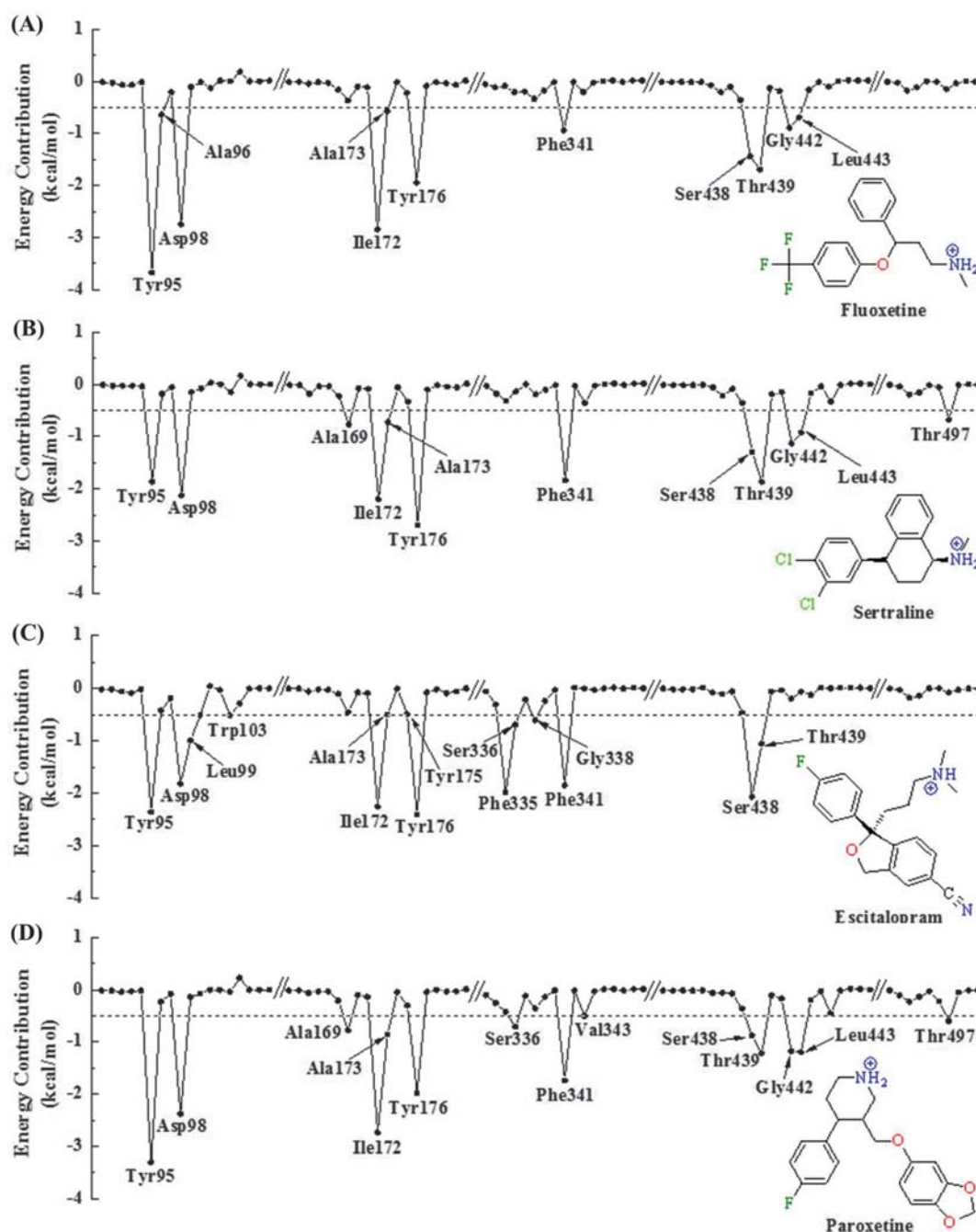

Fig. 3   Per-residue decomposition of binding free energy contributions of 4 SSRI–hSERT complexes.

Representative snapshots of SSRI–hSERT complexes from equilibrated MD trajectories are also shown in Fig. S8, ESI† illustrating the orientations of each SSRI and its interacting residues. However, to fully understand the binding mode of SSRI–hSERT, it is essential to quantitatively distinguish contributions of each amino acid to the drug binding. Thus, plots showing binding free energy contributions of each amino acid were generated by a per-residue free energy decomposition analysis (Fig. 3). To the best of our knowledge, Fig. 3 shows the first reported SSRIs' binding free energy contributions at a per-residue basis.

As illustrated in Fig. 3, there were 11, 12, 14 and 14 residues identified as high contribution ones (with the absolute energy contribution of ≥ 0.5 kcal mol^{-1}) for binding fluoxetine, sertraline, escitalopram and paroxetine respectively. On one hand, energy contributions of different residues to the same SSRI vary greatly (for example, from -0.57 kcal mol^{-1} for Ala173 to -3.68 kcal mol^{-1} for Tyr95 in fluoxetine's binding), and energy contributions of the same residue to different SSRIs also differ significantly (the polar residue Asp98's contributions ranged from -1.83 kcal mol^{-1} for escitalopram to -2.75 kcal mol^{-1} for fluoxetine, as an example). On the other hand, Fig. 3 also infers a certain level of similarity among the 4 studied SSRIs, which inspired us to conduct a deeper exploration of the binding mode shared by 4 SSRIs.

Identifying the binding mode shared by approved SSRIs

Binding mode shared by approved SSRIs to hSERT could provide a useful framework from which novel lead scaffolds can be assessed and discovered.[23] To identify the binding mode, the hierarchical clustering with the Ward algorithm[63] was applied to find hot spot residues from those per-residue binding free energies generated in the previous section. In particular, there were 541 residues with available binding free energy contribution to the 4 studied SSRIs, 296 of which have no contribution (=0 kcal mol^{-1}) to the binding of any studied SSRIs. Then, energy contributions of the remaining 245 residues were used for clustering analysis. As illustrated by the
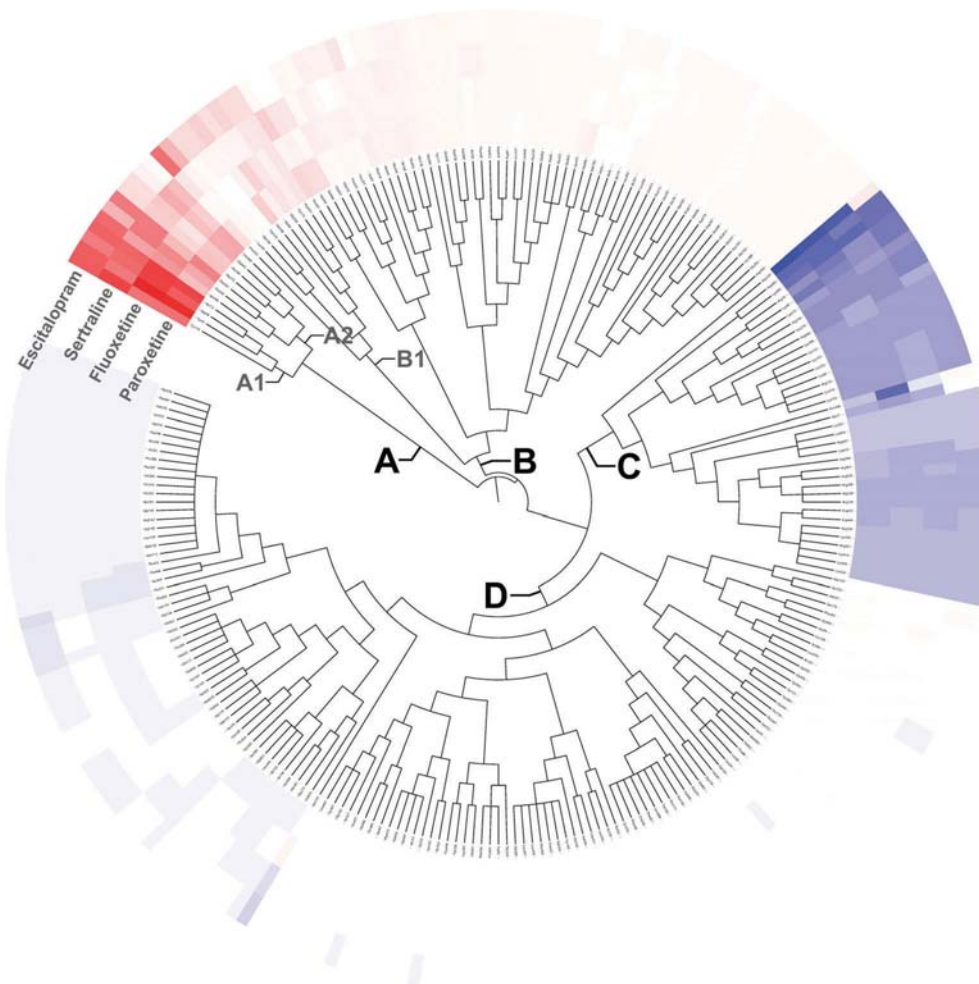

Fig. 4 Hierarchical clustering tree of 245 residues with contributions to at least one studied SSRI in hSERT's binding by their per-residue energy contributions. Per-residue binding free energy contributions favoring SSRI's binding are displayed in red, with the highest contribution set to exact red and lower contributions gradually fading towards white (no contribution). Per-residue energy contributions hampering SSRI's binding are shown in blue, with the highest one set to exact blue and lower ones gradually fading towards white.

This journal is © the Owner Societies 2016

Phys. Chem. Chem. Phys., 2016, 18, 3260–3271 | 3265

hierarchical tree in Fig. 4, 4 distinct residue groups (A, B, C and D) were identified. Binding free energy contributions favoring SSRI's binding were displayed in red, with the highest contribution (-3.68 kcal mol^{-1}) set to exact red and lower contributions gradually fading towards white (contribution = 0 kcal mol^{-1}). Meanwhile, binding free energy contributions hampering SSRI's binding were shown in blue, with the highest one (0.22 kcal mol^{-1}) set to exact blue and lower ones gradually fading towards white. It is necessary to clarify that the absolute value of the highest contribution favoring SSRI's binding (exact red) is 16 times stronger than that hampering the binding (exact blue).

It is clear to see that binding free energy contributions of residues in group A (Tyr95, Asp98, Ala169, Ile172, Ala173, Tyr176, Phe341, Ser438, Thr439, Gly442 and Leu443) are consistently higher across the 4 studied SSRIs in favoring the binding than those in groups B, C and D. For each SSRI, the sum of energy contributions of residues in group A constitutes the primary portion of the total energy (77.04% for fluoxetine, 74.01% for sertraline, 60.19% for escitalopram and 71.73% for paroxetine). Therefore, these 11 residues in hSERT were identified as hot spots for the binding of 4 SSRIs. Moreover, energy contributions of residues in the subgroup A1 (Tyr95, Asp98, Ile172 and Tyr176) are more significant than those in subgroup A2 (Ala169, Ala173, Phe341, Ser438, Thr439, Gly442 and Leu443), and the sum of energy contributions of residues in subgroup A1 consists of 48.55%, 37.68%, 35.34% and 40.87% of total energies for fluoxetine, sertraline, escitalopram and paroxetine, respectively. Thus, residues in subgroups A1 and A2 could be classified as hot spots with "strong" and "relatively strong" contributions.

Moreover, the root mean square fluctuation (RMSF) *versus* the protein residue numbers of hSERT was calculated and illustrated in Fig. S9, ESI.† It is observed that the hot spot residues of hSERT (Tyr95, Asp98, Ala169, Ile172, Ala173, Tyr176, Phe341, Ser438, Thr439, Gly442 and Leu443) show
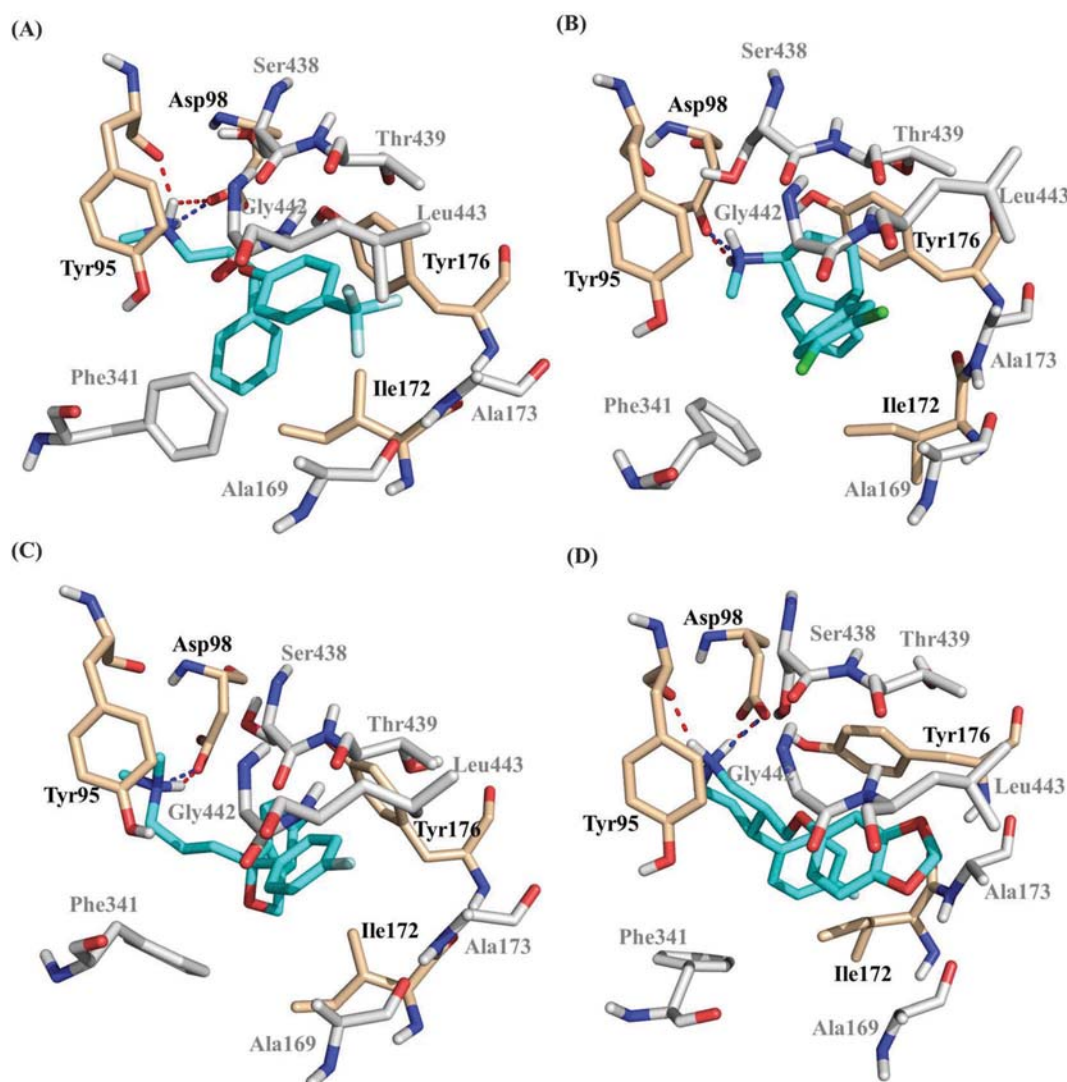

Fig. 5 The binding mode of SSRIs (A) fluoxetine, (B) sertraline, (C) escitalopram and (D) paroxetine to 11 hot spot residues in hSERT. Residues and SSRIs are shown in stick representation, and salt bridges and hydrogen bonds are depicted in blue and red dotted lines, respectively.

relatively rigid behaviors for the studied 4 complexes. The relatively low RMSF values of those residues suggest that SSRI binding could stabilize the key residues located at the drug binding site. This is in accordance with the observed stabilization effect in previous study.[70]

The conformational features of how SSRIs accommodate into 11 hot spot residues are shown in Fig. 5. A pocket was defined by hot spot residues with a slight conformational shift, and all SSRIs fitted the pocket in a resembled orientation. Therefore, the binding mode of SSRI–hSERT recognition was generalized and schematically represented in Fig. 6. As shown, the binding mode was defined by collective hydrophilic and hydrophobic interactions between 3 chemical groups (R1, R2 and R3) and 11 hot spot residues (Tyr95, Asp98, Ala169, Ile172, Ala173, Tyr176, Phe341, Ser438, Thr439, Gly442 and Leu443). As shown in Fig. 5 and Fig. 6, the hot spot residues with strong and relatively strong contributions are illustrated in black and gray color, respectively. Chemical groups in Fig. 6 are highlighted in blue and green. In particular, R1 formed salt-bridge and hydrogen bond interactions with Asp98; R2 interacted with Ala169, Ile172, Tyr176 and Phe341 via hydrophobic contacts; R3 formed hydrophobic interactions with Tyr95, Ala173, Ser438, Thr439, Gly442 and Leu443, and also with Ile172, Tyr176 and Phe341.

Among those 11 identified hot spot residues, 6 (Tyr95, Asp98, Ile172, Tyr176, Phe341 and Ser438) were collectively validated by previous mutagenesis studies[20–22,40,71,72] as sensitive to the 4 approved SSRIs. Co-crystallized structures of SSRIs in hSERT's homolog[37,73] could shed great light on their binding mechanism, but so far no structure of escitalopram in hSERT's homolog has been reported. Based on co-crystallized structures of 3 SSRIs (fluoxetine, sertraline and paroxetine), 7 residues (Tyr95, Asp98, Ile172, Ala173, Tyr176, Phe341 and Gly442) were suggested as primary binding by visualizing interaction distances between SSRIs and LeuBAT.[37] Besides mutagenesis studies and crystal structures, computational methods such as induced fit docking,[20–22,27,28] pharmacophore model[29–31]

and molecular dynamics[32] collectively identified 4 residues (Tyr95, Asp98, Ile172 and Tyr176) as features for 4 SSRIs' binding.[21,22,31,71,72] All primary binding residues found in co-crystallized structures and features identified by computational methods are covered by those 11 hot spot residues of this study. Besides those 6 residues (Tyr95, Asp98, Ile172, Tyr176, Phe341 and Ser438) identified by mutagenesis studies and computational methods, 5 hot spot residues found in this work have not yet been identified by previous studies as common determinants of 4 approved SSRIs in binding hSERT. However, among these 5 hot spots, 2 (Ala173 and Gly442) were suggested to interact with fluoxetine, sertraline and paroxetine,[37] 1 (Thr439) was found as sensitive to fluoxetine[22] and escitalopram,[72] and 2 (Ala169 and Leu443) were only reported to be in close proximity to the cyano group of escitalopram.[21,72] Thus, Ala169, Ala173, Thr439, Gly442 and Leu443 were identified for the first time as common determinants of 4 FDA approved SSRIs treating major depression in binding hSERT.

Besides group A in Fig. 4, group B (especially subgroup B1) represents residues with significant differences in binding free energy contribution. The sum of energy contributions of residues in subgroup B1 (Ala96, Leu99, Gly100, Trp103, Tyr175, Phe335, Ser336, Gly338 and Asp437) consists of 8.09%, 8.60%, 25.41%, and 10.33% of total energies for fluoxetine, sertraline, escitalopram and paroxetine, respectively. In particular, Phe335 and Leu99 were main energy contributors to escitalopram's binding. Consider residue Phe335 as an example, its contribution to escitalopram's binding was relatively strong (-1.99 kcal mol^{-1}), while its contributions to other 3 SSRIs' binding were weaker with the highest contribution to paroxetine (-0.42 kcal mol^{-1}). As illustrated in Fig. S8C (ESI†), the strong contribution of Phe335 may come from its interaction with escitalopram's cyano group which is in the close vicinity of Phe335. Meanwhile, Gly442 and Leu443 showed stronger interactions with fluoxetine, sertraline and paroxetine than with escitalopram, and Ala96 showed a stronger interaction with fluoxetine than with other SSRIs. Understanding energy differences on per-residue basis could
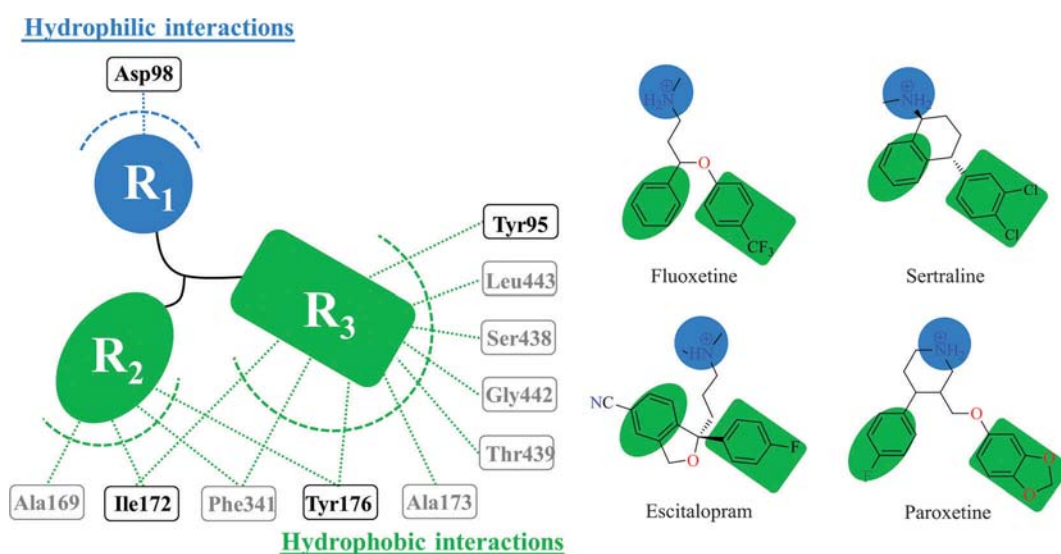

Fig. 6 Schematic representation of the binding mode of the 4 studied SSRIs to hSERT identified in this work.

This journal is © the Owner Societies 2016

Phys. Chem. Chem. Phys., 2016, **18**, 3260–3271 | **3267**

help interpret drug selectivity, which may eventually aid the development of future selective antidepressants.

Group C represents residues with contributions hampering the binding of 4 SSRIs to hSERT. It is necessary to clarify that the absolute value of the highest contribution favoring SSRI's binding (exact red) is 16 times stronger than that hampering the binding (exact blue), which makes the contribution favoring the binding overwhelming. Moreover, Arg104 and Asn368 are identified in Fig. 4 as residues favoring (fluoxetine, sertraline and paroxetine) or hampering (escitalopram) the binding of SSRIs to hSERT.

In silico analysis of drug sensitivity profile on hot spot residues

Analyzing drug sensitive mutation *via* binding free energy. Analysis of the sensitivity profiles could provide an insight into

SSRIs' binding mode.[21] Sensitivity of certain residues to SSRI's binding can be reflected by comparing the difference in energy contributions before and after *in silico* mutation on the corresponding residue. It is easy to understand that mutations on hot spot residues are critical to drug sensitivity. Therefore, this study investigated the influence of hot spot residues-mutation on SSRIs' binding. In particular, 12 single-point mutant complexes were analyzed individually by adding 20 ns of simulation using the assessed wild type model as the starting point (ESI,† Fig. S8). Binding free energies were also calculated (ESI,† Table S1). As a comparison, impacts of hSERT mutations on the binding affinities of SSRIs from previous experimental study[40] are listed in Table S1, ESI.† A significant decrease in K_i from the wild type to the mutant in an experiment[40] was reproduced very

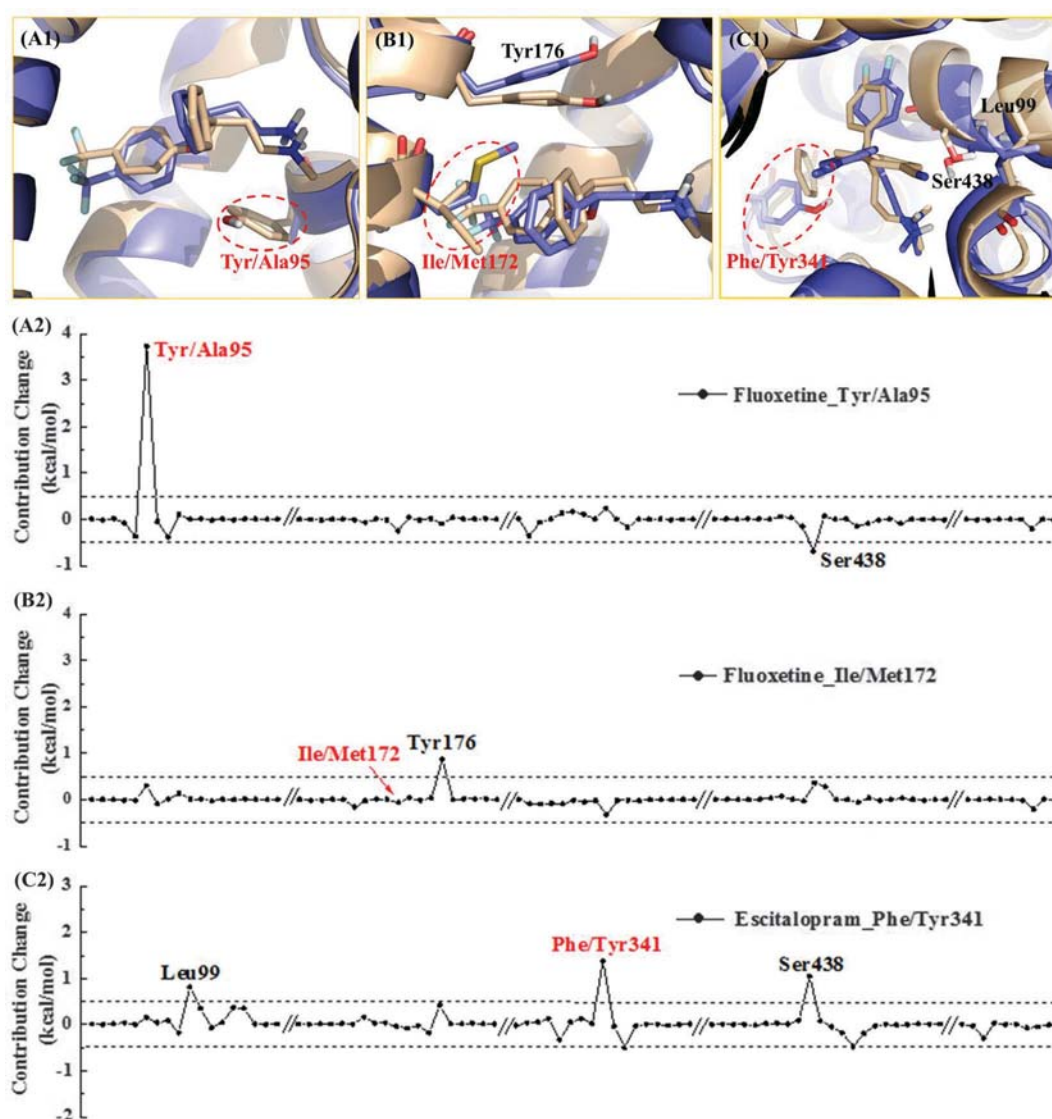Fig. 7 Three mechanisms underlying drug sensitivity induced by mutations on hot spot residues. Structural superimposition of (A1) fluoxetine binding to wild type and Tyr/Ala95 mutant hSERT, (B1) fluoxetine binding to wild type and Ile/Met172 mutant hSERT and (C1) escitalopram binding to wild type and Phe/Tyr341 mutant hSERT. Contribution changes in SSRI's binding (A2–C2) by mutation on hot spot residues measured by the per-residue binding free energy corresponding to A1–C1. Residues affected were shown as a stick representation in wild type (light brown) and mutant (lightblue) models. The mutation residues were highlighted in red dash circles and fonts.

well by $\Delta G_{\text{MM/GBSA}}$, whereas two exceptions (Phe/Tyr341 and Ser/Thr438) from paroxetine's binding were also observed.

Exploring the mechanism of hot spot residue mutation induced drug sensitivity. Drug sensitive mutation on hot spot residues led to conformational changes in hSERT's binding pocket, and orientation shifts of SSRIs to accommodate into the pocket were observed (Fig. 7(A1–C1) and Fig. S9, ESI†). This structural rearrangement further led to changes in the binding free energy contribution of each amino acid (Fig. 7(A2–C2) and Fig. S10, ESI†). By correlating mutations on hot spot residues with changes in binding free energy contribution, 3 mechanisms underlining mutation-induced drug sensitivity were summarized.

In the first mechanism, mutation-induced drug sensitivity comes directly from a significant binding free energy contribution loss in mutational residues. Taking Tyr/Ala95 of fluoxetine's binding as an example, in spite of an increase (-0.69 kcal mol^{-1}) in Ser438, the binding free energy contribution was dramatically decreased (3.73 kcal mol^{-1}) in the mutational residue Tyr/Ala95, which resulted in unfavorable binding (Fig. 7(A2)). The detailed structural rearrangements (Fig. 7(A1)) further clarified that reduction in the side chain size from Try to Ala was the main reason of mutation-induced drug sensitivity.

In the second mechanism, mutation-induced drug sensitivity originates from binding free energy contribution loss in residues other than the mutational one. Taking Ile/Met172 of fluoxetine's binding as an example, in contrast to the unnoticeable energy change in the mutational residue Ile/Met172, binding free energy contribution was decreased by 0.87 kcal mol^{-1} in Tyr176 leading to unfavorable binding (Fig. 7(B2)). As shown in Fig. 7(B1), a clear increase in the distance between fluoxetine and its interacting residue Tyr176 was induced by Ile/Met172 mutation, which resulted in the decrease in Tyr176's binding free energy contribution.

In the third mechanism, mutation-induced drug sensitivity comes from binding free energy contribution loss from both mutational and other residues. Taking Phe/Tyr341 of escitalopram's binding as an example, besides a great decrease by 1.14 kcal mol^{-1} in the mutational residue Phe/Tyr341, binding free energy contribution was also decreased by 0.82 and 1.05 kcal mol^{-1} in Leu99 and Ser438, respectively (Fig. 7(C2)). Phe/Tyr341 mutation induced a clear structural rotation of escitalopram in the binding pocket, and led to unfavorable interactions between the drug and two other residues (Leu99 and Ser438 in Fig. 7(C1)), which contributed to the mutation-induced drug sensitivity.

As shown in Fig. 7 and Fig. S9 and S10, ESI† all residues with significant changes in binding free energy contribution between the mutant and wild type hSERT were from those 11 hot spot residues or residues in their close vicinity, which further validates the binding mode of SSRIs' binding to hSERT identified in this study.

Conclusion

In this study, identification of the inhibitory mechanism from 4 approved SSRIs treating major depression was carried out by integrating multiple computational methods. A recently reported template dDAT was successfully adopted to generate the homology model of hSERT, and the binding mode shared by the 4 studied SSRIs was identified by hierarchically clustering per-residue binding free energies of 245 residues with contributions to at least one studied SSRI in hSERT's binding. The identified binding mode was defined by interactions between SSRIs and 11 hot spot residues (Tyr95, Asp98, Ala169, Ile172, Ala173, Tyr176, Phe341, Ser438, Thr439, Gly442 and Leu443) in hSERT. 6 out of these 11 hot spot residues were validated by previous mutagenesis studies or pharmacophore models. 5 hot spot residues (Ala169, Ala173, Thr439, Gly442 and Leu443) found in this work have not yet been identified as common determinants of all 4 studied SSRIs in binding hSERT. In the last section of this study, changes in SSRIs' binding induced by mutation on hot spot residues were further explored, and 3 mechanisms underlining their drug sensitivity were summarized. The binding mode identified in this study provided significant insights into the inhibitory mechanism of approved SSRIs, which could be utilized as a useful framework for assessing and discovering novel lead scaffolds.

Acknowledgements

References

1 Y. S. Nikolova, K. C. Koenen, S. Galea, C. M. Wang, M. L. Seney, E. Sibille, D. E. Williamson and A. R. Hariri, *Nat. Neurosci.*, 2014, **17**, 1153–1155.

2 C. Kaplan and Y. Zhang, *J. Ment. Health Policy Econ.*, 2012, **15**, 171–178.

3 F. Lopez-Munoz and C. Alamo, *Curr. Pharm. Des.*, 2009, **15**, 1563–1586.

4 M. P. Cruz, *P&T: A Peer-Reviewed Journal for Formulary Management*, 2012, **37**, 28–31.

5 H. Tagashira, M. S. Bhuiyan, N. Shioda and K. Fukunaga, *Life Sci.*, 2014, **95**, 89–100.

6 F. C. Arslan, E. K. Uysal, E. Ozkorumak and A. Tiryaki, *Gen. Hosp. Psychiatry*, 2015, **37**, e371–e372.

7 S. C. Leiser, D. Iglesias-Bregna, L. Westrich, A. L. Pehrson and C. Sanchez, *J. Psychopharmacol*, 2015, **29**, 1092–1105.

8 C. I. Petersen and L. J. DeFelice, *Nat. Neurosci.*, 1999, **2**, 605–610.

9 F. Zhu, Z. Shi, C. Qin, L. Tao, X. Liu, F. Xu, L. Zhang, Y. Song, X. Liu, J. Zhang, B. Han, P. Zhang and Y. Chen, *Nucleic Acids Res.*, 2012, **40**, D1128–1136.

10 D. Marazziti, P. Landi, S. Baroni, F. Vanelli, N. Bartolommei, M. Picchetti and L. Dell'Osso, *Curr. Drug Targets*, 2013, **14**, 522–530.

11 A. Caspi, A. R. Hariri, A. Holmes, R. Uher and T. E. Moffitt, *Am. J. Psychiatry*, 2010, **167**, 509–527.

12 F. Artigas, *ACS Chem. Neurosci.*, 2013, **4**, 5–8.

13 G. I. Papakostas, *J. Clin. Psychiatry*, 2009, **70**(suppl. 6), 16–25.

14 M. H. Flight, *Nat. Rev. Drug Discovery*, 2013, **12**, 578–579.

15 M. J. Millan, *Neurotherapeutics*, 2009, **6**, 53–77.

16 E. Gulbins, M. Palmada, M. Reichel, A. Luth, C. Bohmer, D. Amato, C. P. Muller, C. H. Tischbirek, T. W. Groemer, G. Tabatabai, K. A. Becker, P. Tripal, S. Staedtler, T. F. Ackermann, J. van Brederode, C. Alzheimer, M. Weller, U. E. Lang, B. Kleuser, H. Grassme and J. Kornhuber, *Nat. Med.*, 2013, **19**, 934–938.

17 R. E. Horton, D. M. Apple, W. A. Owens, N. L. Baganz, S. Cano, N. C. Mitchell, M. Vitela, G. G. Gould, W. Koek and L. C. Daws, *J. Neurosci.*, 2013, **33**, 10534–10543.

18 S. L. Diaz, S. Doly, N. Narboux-Neme, S. Fernandez, P. Mazot, S. M. Banas, K. Boutourlinsky, I. Moutkine, A. Belmer, A. Roumier and L. Maroteaux, *Mol. Psychiatry*, 2012, **17**, 154–163.

19 P. Bonaventure, L. Kelly, L. Aluisio, J. Shelton, B. Lord, R. Galici, K. Miller, J. Atack, T. W. Lovenberg and C. Dugovic, *J. Pharmacol. Exp. Ther.*, 2007, **321**, 690–698.

20 J. Andersen, O. Taboureau, K. B. Hansen, L. Olsen, J. Egebjerg, K. Stromgaard and A. S. Kristensen, *J. Biol. Chem.*, 2009, **284**, 10276–10284.

21 J. Andersen, L. Olsen, K. B. Hansen, O. Taboureau, F. S. Jorgensen, A. M. Jorgensen, B. Bang-Andersen, J. Egebjerg, K. Stromgaard and A. S. Kristensen, *J. Biol. Chem.*, 2010, **285**, 2051–2063.

22 J. Andersen, N. Stuhr-Hansen, L. G. Zachariassen, H. Koldso, B. Schiott, K. Stromgaard and A. S. Kristensen, *Mol. Pharmacol.*, 2014, **85**, 703–714.

23 A. Yan, L. Wang, S. Xu and J. Xu, *Drug Discovery Today*, 2011, **16**, 260–269.

24 A. Yamashita, S. K. Singh, T. Kawate, Y. Jin and E. Gouaux, *Nature*, 2005, **437**, 215–223.

25 S. K. Singh, C. L. Piscitelli, A. Yamashita and E. Gouaux, *Science*, 2008, **322**, 1655–1661.

26 H. Koldso, A. B. Christiansen, S. Sinning and B. Schiott, *ACS Chem. Neurosci.*, 2013, **4**, 295–309.

27 L. Celik, S. Sinning, K. Severinsen, C. G. Hansen, M. S. Moller, M. Bols, O. Wiborg and B. Schiott, *J. Am. Chem. Soc.*, 2008, **130**, 3853–3865.

28 K. Severinsen, H. Koldso, K. A. Thorup, C. Schjoth-Eskesen, P. T. Moller, O. Wiborg, H. H. Jensen, S. Sinning and B. Schiott, *Mol. Pharmacol.*, 2014, **85**, 208–217.

29 O. M. Ghoneim, D. A. Ibrahim, I. M. El-Deeb, S. H. Lee and R. G. Booth, *Bioorg. Med. Chem. Lett.*, 2011, **21**, 6714–6723.

30 M. Gabrielsen, R. Kurczab, A. W. Ravna, I. Kufareva, R. Abagyan, Z. Chilmonczyk, A. J. Bojarski and I. Sylte, *Eur. J. Med. Chem.*, 2012, **47**, 24–37.

31 Z. L. Zhou, H. L. Liu, J. W. Wu, C. W. Tsao, W. H. Chen, K. T. Liu and Y. Ho, *Chem. Biol. Drug Des.*, 2013, **82**, 705–717.

32 A. M. Jorgensen, L. Tagmose, A. M. Jorgensen, K. P. Bogeso and G. H. Peters, *ChemMedChem*, 2007, **2**, 827–840.

33 S. Sinning, M. Musgaard, M. Jensen, K. Severinsen, L. Celik, H. Koldso, T. Meyer, M. Bols, H. H. Jensen, B. Schiott and O. Wiborg, *J. Biol. Chem.*, 2010, **285**, 8363–8374.

34 K. Severinsen, J. F. Kraft, H. Koldso, K. A. Vinberg, R. B. Rothman, J. S. Partilla, O. Wiborg, B. Blough, B. Schiott and S. Sinning, *ACS Chem. Neurosci.*, 2012, **3**, 693–705.

35 B. A. Merchant and J. D. Madura, *J. Mol. Graphics Modell.*, 2012, **38**, 1–12.

36 A. Penmatsa, K. H. Wang and E. Gouaux, *Nature*, 2013, **503**, 85–90.

37 H. Wang, A. Goehring, K. H. Wang, A. Penmatsa, R. Ressler and E. Gouaux, *Nature*, 2013, **503**, 141–145.

38 A. Penmatsa, K. H. Wang and E. Gouaux, *Nat. Struct. Mol. Biol.*, 2015, **22**, 506–508.

39 M. Gabrielsen, A. W. Ravna, K. Kristiansen and I. Sylte, *J. Mol. Model.*, 2012, **18**, 1073–1085.

40 L. Sorensen, J. Andersen, M. Thomsen, S. M. Hansen, X. Zhao, A. Sandelin, K. Stromgaard and A. S. Kristensen, *J. Biol. Chem.*, 2012, **287**, 43694–43707.

41 K. Arnold, L. Bordoli, J. Kopp and T. Schwede, *Bioinformatics*, 2006, **22**, 195–201.

42 R. A. Laskowski, M. W. MacArthur, D. S. Moss and J. M. Thornton, *J. Appl. Crystallogr.*, 1993, **26**, 283–291.

43 *The PyMOL Molecular Graphics System, version 1.3*, Schrödinger, LLC.

44 Glide, *version 5.5*, Schrödinger, LLC, New York, 2009.

45 S. Jo, T. Kim, V. G. Iyer and W. Im, *J. Comput. Chem.*, 2008, **29**, 1859–1865.

46 S. Jo, J. B. Lim, J. B. Klauda and W. Im, *Biophys. J.*, 2009, **97**, 50–58.

47 E. L. Wu, X. Cheng, S. Jo, H. Rui, K. C. Song, E. M. Davila-Contreras, Y. Qi, J. Lee, V. Monje-Galvan, R. M. Venable, J. B. Klauda and W. Im, *J. Comput. Chem.*, 2014, **35**, 1997–2004.

48 W. L. Jorgensen, J. Chandrasekhar, J. D. Madura, R. W. Impey and M. L. Klein, *J. Chem. Phys.*, 1983, **79**, 926–935.

49 D. A. Case, J. T. Berryman, R. M. Betz, Q. Cai, D. S. Cerutti, T. E. CheathamIII, T. A. Darden, R. E. Duke, H. Gohlke, A. W. Goetz, S. Gusarov, N. Homeyer, P. Janowski, J. Kaus, I. Kolossváry, A. Kovalenko, T. S. Lee, S. LeGrand, T. Luchko, R. Luo, B. Madej, K. M. Merz, F. Paesani, D. R. Roe, A. Roitberg, C. Sagui, R. Salomon-Ferrer, G. Seabra, C. L. Simmerling, W. Smith, J. Swails, R. C. Walker, J. Wang, R. M. Wolf, X. Wu and P. A. Kollman, *AMBER 14*, University of California, San Francisco, 2014.

50 V. Hornak, R. Abel, A. Okur, B. Strockbine, A. Roitberg and C. Simmerling, *Proteins*, 2006, **65**, 712–725.

51 C. J. Dickson, B. D. Madej, A. A. Skjevik, R. M. Betz, K. Teigen, I. R. Gould and R. C. Walker, *J. Chem. Theory Comput.*, 2014, **10**, 865–879.

52 I. S. Joung and T. E. Cheatham, *J. Phys. Chem. B*, 2008, **112**, 9020–9041.

53 J. Wang, R. M. Wolf, J. W. Caldwell, P. A. Kollman and D. A. Case, *J. Comput. Chem.*, 2004, **25**, 1157–1174.

54 C. I. Bayly, P. Cieplak, W. Cornell and P. A. Kollman, *J. Phys. Chem.*, 1993, **97**, 10269–10280.

55 J. Wang, W. Wang, P. A. Kollman and D. A. Case, *J. Mol. Graphics Modell.*, 2006, **25**, 247–260.

56 M. J. Frisch, H. B. Schlegel, G. E. Scuseria, M. A. Robb, J. R. Cheeseman, G. Scalmani, V. Barone, B. Mennucci, G. A. Petersson, H. Nakatsuji, M. Caricato, X. Li, H. P. Hratchian, A. F. Izmaylov, J. Bloino, G. Zheng, J. L. Sonnenberg, M. Hada, M. Ehara, K. Toyota, R. Fukuda, J. Hasegawa, M. Ishida, T. Nakajima, Y. Honda, O. Kitao, H. Nakai, T. Vreven, J. A. Montgomery Jr, J. E. Peralta, F. Ogliaro, M. Bearpark, J. J. Heyd, E. Brothers, K. N. Kudin, V. N. Staroverov, R. Kobayashi, J. Normand, K. Raghavachari, A. Rendell, J. C. Burant, S. S. Iyengar, J. Tomasi, M. Cossi, N. Rega, J. M. Millam, M. Klene, J. E. Knox, J. B. Cross, V. Bakken, C. Adamo, J. Jaramillo, R. Gomperts, R. E. Stratmann, O. Yazyev, A. J. Austin, R. Cammi, C. Pomelli, J. W. Ochterski, R. L. Martin, K. Morokuma, V. G. Zakrzewski, G. A. Voth, P. Salvador, J. J. Dannenberg, S. Dapprich, A. D. Daniels, Ö. Farkas, J. B. Foresman, J. V. Ortiz, J. Cioslowski and D. J. Fox, *Gaussian 09*, Gaussian, Inc., Wallingford, CT, 2009.

57 T. Darden, D. York and L. Pedersen, *J. Chem. Phys.*, 1993, **98**, 10089–10092.

58 L. Larini, R. Mannella and D. Leporini, *J. Chem. Phys.*, 2007, **126**, 104101.

59 P. A. Kollman, I. Massova, C. Reyes, B. Kuhn, S. Huo, L. Chong, M. Lee, T. Lee, Y. Duan, W. Wang, O. Donini, P. Cieplak, J. Srinivasan, D. A. Case and T. E. Cheatham 3rd, *Acc. Chem. Res.*, 2000, **33**, 889–897.

60 I. Massova and P. A. Kollman, *Perspect. Drug Discovery Des.*, 2000, **18**, 113–135.

61 J. Weiser, P. S. Shenkin and W. C. Still, *J. Comput. Chem.*, 1999, 217–230.

62 S. Tippmann, *Nature*, 2015, **517**, 109–110.

63 J. H. Ward Jr, *J. Am. Stat. Assoc.*, 1963, **58**, 236–244.

64 I. Letunic and P. Bork, *Bioinformatics*, 2007, **23**, 127–128.

65 J. Zeng, L. Duan, J. Z. Zhang and Y. Mei, *J. Comput. Chem.*, 2013, **34**, 847–853.

66 J. Wang, P. Morin, W. Wang and P. A. Kollman, *J. Am. Chem. Soc.*, 2001, **123**, 5221–5230.

67 C. M. Reyes and P. A. Kollman, *J. Mol. Biol.*, 2000, **297**, 1145–1158.

68 H. Gohlke and D. A. Case, *J. Comput. Chem.*, 2004, **25**, 238–250.

69 B. L. Kormos, Y. Benitex, A. M. Baranger and D. L. Beveridge, *J. Mol. Biol.*, 2007, **371**, 1405–1419.

70 Z. Zhang, V. Martiny, D. Lagorce, Y. Ikeguchi, E. Alexov and M. A. Miteva, *PLoS One*, 2014, **9**, e110884.

71 S. Tavoulari, L. R. Forrest and G. Rudnick, *J. Neurosci.*, 2009, **29**, 9635–9643.

72 H. Koldso, K. Severinsen, T. T. Tran, L. Celik, H. H. Jensen, O. Wiborg, B. Schiott and S. Sinning, *J. Am. Chem. Soc.*, 2010, **132**, 1311–1322.

73 Z. Zhou, J. Zhen, N. K. Karpowich, C. J. Law, M. E. Reith and D. N. Wang, *Nat. Struct. Mol. Biol.*, 2009, **16**, 652–657.